ARTICLE

Effect of Rake Angle on DTMB Marine Propeller

Muhammad Suleman Sadiq [1], Adil Loya [2] (iD), Imran Mushtaque [2], Wasim Akram [1]*

[1] *Department of Naval Architecture, National University of Sciences and Technology, Karachi, Sindh, Pakistan*
[2] *Department of Mechanical Engineering, National University of Sciences and Technology, Karachi, Sindh, Pakistan*

ABSTRACT

The marine propeller typically functions within the flow field generated by a water vehicle. Investigations into the geometric parameters of the propeller are commonly conducted under open-water conditions as simultaneously simulating both vehicle and propeller holds several computational challenges. While during operation, this propellant device must face several forces like gravity, hydrodynamic load, and centrifugal force, which cause different problems like cavitation and structural failure, etc. Since these issues affect performance, it necessitates comprehensive analysis. In this study, hydrodynamic analysis is performed by using commercial software STAR CCM+. In hydrodynamic analysis, the effect of the rake angles –5°, 5°, 10° and 15° on hydrodynamic coefficients and efficiency of the DTMB 4119 in the open water is analyzed using Computational Fluid Dynamics (CFD) and the control volume approach. The Shear Stress Transport (SST) k-ω turbulence model is used in Computational Fluid Dynamics (CFD) simulation. Hydrodynamic analysis reveals that the rake angles 5° and 10° cause the open water efficiency of David Taylor Model Basin (DTMB) 4119 to improve by 0.4 to 1.32% with exception of the rake angles –5° and 15°, which possess different effects on efficiency. The angle –5° causes a decrease in propeller efficiency under heavy loading situations (low advance coefficient) apart from a minor fluctuation at light loading conditions (high advance coefficient), while the angle 15° produces a drop in efficiency by higher advance ratios but little variation at lower advance ratios.

Keywords: DTMB 4119; Marine Propeller; Rake Angle; Open Water Performance; Unsteady Solution; Hydrodynamic Analysis

1. Introduction

A ship is a huge vessel that moves across expansive bodies of water, particularly the oceans, with the primary objective of transporting individuals or commodities for a diverse range of applications, including defense, scientific investigation, and commercial fishing. Regardless of its mass, its ability to move is entertained by a phenomenon referred to as propulsion. The possibility of this process is made possible by a mechanical device referred to as a propeller[1]. Marine propellers perform a vital function within the maritime sector and shipping operations. In present days, the propellers of different vessels come in a variety of forms, including open, podded, ducted and azimuthing propellers. Several studies have been conducted on multiple impacts of propeller design, including hydrodynamics, hydro-elastic, and hydro-acoustic performance of marine propellers, due to the growing significance of propellers. The investigation of marine propellers located behind the hull remains challenging in practical scenarios owing to the existence of a significantly disrupted wake field. Consequently, the open water performance method is commonly employed for evaluating the hydrodynamic effectiveness of marine propellers. In the open water analysis, the purpose is to examine the efficiency of the propeller in the absence of the hull. This involves analyzing the relationship between the coefficients of thrust and torque and the flow advance coefficients[2]. Within the maritime sector, it is frequently advantageous to assess the performance attributes of a propulsion system using three parameters: the Thrust Coefficient (K_T), the Torque Coefficient (K_Q), and the Efficiency (η). In order to effectively illustrate the hydrodynamic performance of the propeller, it is customary to graphically represent the trio of coefficients (K_T, K_Q, η) in relation to the Advance Ratio (J)[3]. The analytical formulae for calculating parameters of open water hydrodynamic parameters of marine propellers are given below.

$$J = \frac{V_A}{ND} \qquad (1)$$

$$K_T = \frac{T}{\rho N^2 D^4} \qquad (2)$$

$$K_Q = \frac{Q}{\rho N^2 D^5} \qquad (3)$$

$$\eta_\circ = \frac{P_T}{P_Q} = \frac{TV_A}{2\pi NQ} = \frac{JK_T}{2\pi K_Q} \qquad (4)$$

Where, V_A is the propeller forward speed relative to the fluid medium (m s^{-1}), N is the rotational speed of the propeller (rev s^{-1}) and D is the diameter of the propeller (m), T thrust force (N), Q is Torque (Nm), P_T is the produced power and P_Q is the consumed power.

1.1. Hydrodynamic of Marine Propeller

Cho and Lee[4] devised a computational technique aimed at optimizing the configuration of a blade for augmentation of hydrodynamic performance of the propeller. The efficiency of propellers was determined by employing the lifting line (LL) theory, specifically the vortex lattice method, as well as the lifting surface (LS) theory, called the panel method. The former technique is characterized by its one-dimensional nature, whereas the latter technique is distinguished by its 2D nature. Lerbs[5] introduced the lifting line technique, which takes into account the lift generated by the vortex formed around the hypothetical spiral paths generated by the rotating propeller. On the other hand, the lifting surfaces method focuses on the 2D vortices present on the surfaces of the blades[6]. Gaggero and Brizzolara[7] employed the panel method for optimizing the design of a propeller for high-speed vessels, focusing on enhancing efficiency and reducing cavitation. In a separate investigation[8], a comparative analysis was conducted on two distinct propellers, namely the SEIUN-MARU highly skewed propeller and DTMB 4119, utilizing both LS and CFD methodologies. The researchers reached the conclusion that CFD methods can be effectively employed as a robust tool for preliminary design.

The study conducted by Krasilnikov, Sun and Hasel[9] examined the impact of scale on the properties of marine propellers. The researchers utilized the Reynolds Average Navier Stokes (RANS) method and specifically concentrated on the impacts of skew angle, hydrodynamic loading of the propeller, and area ratio of blade area. The analysis performed by Funeno[10] focused on the analysis of unsteady flow patterns surrounding a propeller with high skew angle in the presence of non-uniform inflow. Amoraritei[11] conducted a numerical investigation on the hydrodynamic

performance and flow properties of conventional propellers and azimuth thrusters. The performance of the azimuth thruster's propeller was affected by numerous interactions occurring between the propeller, gondola, and strut. The geometric characteristics of the propeller, gondola, and strut were already established, and the issue at hand was addressed by employing a three-dimensional model and the commercial software FLUENT. In their study, Ebrahimi, Seif and Nouri-Borujerdi[12] conducted a numerical analysis on the turbulent flow of a DTMB 4119 propeller with a diameter of 0.3048 m. This analysis was performed using the RANS method in the FLUENT software, allowing for the estimation of the propeller's hydrodynamic efficiency.

1.2. Hydrodynamic Performance of Marine Propeller

Yari and Ghassemi[13] calculated the hydrodynamic parameters of an SPP-841 propeller through simulations using the Boundary Element Method (BEM). The simulations were conducted at a velocity of 3.13 m s^{-1} and covered an advance coefficients range of 0.4 to 1.3. The calculated parameters were subjected to validation, revealing slight deviations in the efficiency values. Boumediene et al.[14] utilized ANSYS FLUENT 14.0 to calculate the thrust force and torque exerted on the Seiun Maru propeller, which exhibited a high degree of skewness. They further assessed the propeller's open water performance by examining the thrust and torque coefficients across a range of advance coefficients from 0.1 to 1.0. The efficiency of a system is observed to decrease under heavy load conditions but exhibits an increase when the load is reduced to a lighter condition.

Saha, Maruf and Hasan[15] conducted hydrodynamic analysis on a B-series marine propeller with four blades and a diameter of 1.6 m. CFD simulations were employed to investigate the propeller's efficiency. The researchers validated their methodology and found that the K_T and K_Q exhibited a decrease as the J increased. The efficiency trend exhibits a non-linear pattern. Guo et al.[16] employed the CFD method to predict the hydrodynamic parameters of a propeller. An analysis was conducted on two propellers, namely the ONRT and the DTMB 5415 propellers. An observation was made regarding the deviation of the DTMB 5415 efficiency from the Experimental Fluid Dynamics (EFD) data within the advance ratio range of 0.6 to 1. Bouregba et al.[17] conducted open water hydrodynamic analysis on propellers from the Wageningen B series, specifically those with 4, 5, and 6 blades. The analysis was performed using the ANSYS-FLUENT software. The utilization of a propeller having 6 blades was suggested as an optimal choice for open water flows. The numerical analysis conducted by Hu, Huang and Hong[18] examined the transient thrust force and moment of the propeller DTMB 4119 in a viscous flow. The propeller under consideration demonstrated effective performance under conditions of uniform inflow.

Huang et al.[19] utilized the FLUENT module of Ansys software to conduct numerical simulations on the relation between the propeller's advance ratio, coefficients of thrust and torque, as well as the efficiency of supplementary thrust fins. The rake angle of the ship propeller is a prominent geometric parameter that exerts a substantial influence on the marine propeller's hydrodynamic and hydro-acoustic characteristics[12]. The observed skew angle effect has also been shown to possess the capability of predicting hydrodynamic efficiency of the marine propeller within the constraints of the cavitation problem. This study did not take into account the optimization of the diameter, number of blades as well as material selection[20]. The method employed by Mirjalili, Lewis and Mirjalili[20]. was utilized for the purpose of shape optimization of a marine propeller, with the objective of maximizing efficiency and minimizing cavitation. This study also examined the impact of Revolution Per Minute (RPM) and the quantity of blades on both objectives.

The propeller in an open water condition was modelled by Martínez-Calle et al.[21] using the standard $k - \omega$ turbulence model. While the findings of the study were generally deemed satisfactory, it is worth noting that the average margin of error in the estimation of propeller moment stood at 30%. The propeller was modelled by Watanabe et al.[22] under both steady and transient conditions, employing the standard $k - \omega$ turbulence model. The acquired outcomes exhibited a high level of compatibility with the EFD findings, with an average thrust pre-

diction error of 15%. Rhee and Koutsavdis[23] employed a 2D simulation to model the flow characteristics surrounding a propeller. The standard $k - \omega$ turbulence model was utilized for this purpose. It is worth noting that the authors reported an error percentage of 13% in their results. There have been numerous studies to predict the performance of conventional propellers and propellers with high skew angles using CFD methodology. The skew angle is a commonly studied parameter in literature, as demonstrated by the works of Abdel-Maksoud et al. and Ghasemi[24], where its impact on the performance of the propeller was examined. The findings of these studies suggest that the utilization of high-skewed propellers results in a greater reduction of vibrations caused by the propeller on the entire body, while also improving performance characteristics.

The sliding mesh method is a transient CFD modelling technique employed to simulate the behaviour of rotating components. In their study, Krasilnikov, Ponkratov and Crepier[25] examine the application of RANS and panel methods in simulating propellers in open water conditions. This study utilizes RANS computation to evaluate the Moving Reference Frame (MRF) method's effectiveness in determining coefficients of thrust and torque along with open water efficiency.

After reviewing detailed literature, it is observed that most of the hydrodynamic analysis of marine propellers in uniform flow are steady instead of transient. The geometrical parameters of marine propellers like skew and rake angles have considerable effect on its hydrodynamic performance. It is now known from literature that different models of marine propellers exhibit distinctive responses to rake angle modification in various conditions of flow such as uniform or non-uniform and cavitating or non-cavitating, at different advance coefficients and pitch ratios (P/D). In addition to this, to the best of the knowledge, it is scarce to witness a single study that presents the detailed parametric changes on hydrodynamic performance by implementation of rake angle on DTMB4119. Therefore, this study presents the effect of rake angle modification on the hydrodynamic performance of the propeller.

2. Methods

2.1. Computational Fluid Dynamic (CFD) Simulation

2.1.1. CAD Model of Propeller

In this research study, DTMB 4119 is chosen for hydrodynamic analysis by using Computational Fluid Dynamics (CFD) due to increased availability of experimental results of this model of marine propeller. CFD simulations are performed to generate the hydrodynamic performance curves of DTMB 4119 as shown in **Figure 1**. This model is right-handed and three-bladed with variable pitch marine propeller. It was designed at the David Taylor Model Basin of the United States. The specific dimensions of this model of propeller are tabulated in **Table 1**.
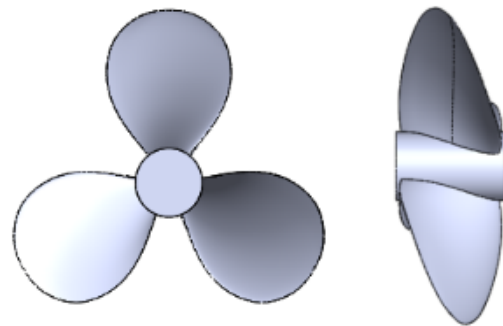

Figure 1. Front and side view of DTMB 4119.

Table 1. Particulars of DTMB 4119.

Number of blades	3
Diameter (D)	0.250 m
Blade section	NACA 66 (a = 0.8)
Pitch ratio at r/R = 0.7	1.0839
Rake angle (°)	0°
Skew angle (°)	0°
Hub length	0.086 m
Hub diameter	0.050 m
Rotation direction	Right

2.1.2. Generation of Computational Fluid Domain

The computational domain for this CFD simulation is basically divided into two portions, one is the rotary domain, and the second one is the static domain. After importing the step file of the DTMB 4119 CAD Model into STAR CCM +, both domains are created by taking dimen-

sions from the center of DTMB 4119. The rotary domain is a cylindrical domain having a diameter of 1.1 D and a length of 1D as shown in **Figure 2**. This domain is symmetrically distributed around the propeller center. The static domain is a blocked domain having a square cross-section of (4 × 4) D to avoid the effect of boundaries and the overall length of this domain is 10D to prevent reverse flow which is divided in such a way that inlet and outlet sides are at distances of 2D and 8D respectively from the center of the propeller as shown in **Figure 2**.
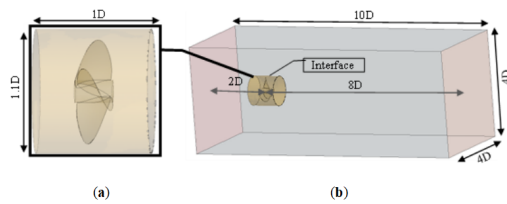

Figure 2. Computational domain: (**a**) rotary domain, (**b**) static domain for CFD analysis.

2.1.3. Mesh Generation

Mesh generation is the most technical aspect of CFD analysis because the accuracy of results, convergence solution, and time taken by the solver depend on the way of generating mesh. So, to make sure the results accuracy and speedy convergence of solution, different mesh sizes are utilized for both domains. Star CCM+, like other software, deals with structured mesh and unstructured mesh to divide the fluid region. Structured mesh encompasses trimmed cell, extruder, and prism layer mesher while unstructured mesh includes polyhedral and tetrahedral.

A Trimmed Cell Mesher and surface remesher without prism layer are used for the static domain and volumetric control is also applied for refinement of mesh cells around the propeller wake region contained in this domain as shown in **Figure 3**. For the rotary domain, polyhedral mesh, and surface remesher with prism layer are utilized. The rotary domain is treated as a moving mesh zone. The purpose of applying polyhedral mesher on this domain is that it is less diffusive with more stable numerically and above all these facts, it has more accuracy than the equivalent tetrahedral mesher having five times fewer cells. For the implementation of mesh refinement around propeller and wake region in this domain, surface and volumetric control are respectively applied
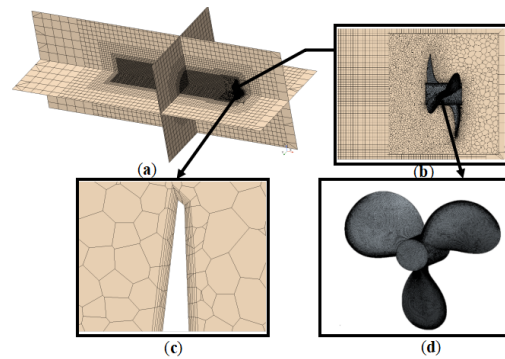
as shown in **Figure 3**.

Figure 3. Visualization of meshing: (**a**) trimmed cell mesher for static domain with refinement at wake region of propeller, (**b**) polyhedral mesher for rotary domain, (**c**) visualization of prism layers around the propeller, (**d**) Refined meshing at propeller leading edges.

2.1.4. Mesh Independence Study

To analyze the effect of mesh cells on the CFD simulation results, a mesh independence study is carried out by ascertaining any parameter for different numbers of mesh cells. This study helps us to know about the minimum number of mesh elements which give us accurate results. Since this CFD analysis contains two regions for mesh operations, element sizes of both mesh regions are varied. The base sizes are varied from 0.25 to 0.02 m for the static mesh region and from 0.125 to 0.01 m for the rotary mesh region. As the base sizes decrease, the cell counts increase and as a result, the mesh density increases from coarse to very fine as shown in **Figure 4**. For the mesh independence study, the moment coefficient is calculated for different cell counts as shown in **Table 2**.
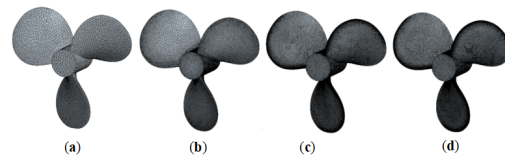

Figure 4. Mesh density: (**a**) coarse mesh, (**b**) medium mesh, (**c**) fine mesh, and (**d**) very fine mesh.

It is observed that the value of the moment coefficient is converged at base sizes of 0.022 m for the static region mesh and 0.011 m for the rotary mesh region with a cell count of 1.72 million as shown in **Figure 5**. So, after doing the mesh independence study, it is decided that base sizes of 0.022 and 0.011 will be used for further sim-

Table 2. Mesh independence study.

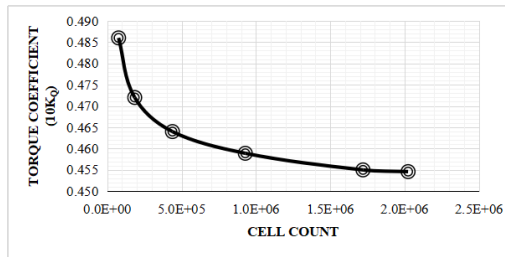| Serial No.	Base Size	Base Size	Cell Count	Moment Coefficient	% Error	Grid Density
1	0.25	0.125	7.63E+04	0.486	17.39	Coarse
2	0.125	0.0625	1.85E+05	0.472	14.01	Slightly coarse
3	0.0625	0.03125	4.38E+05	0.464	12.08	Medium
4	0.03125	0.015625	9.28E+05	0.459	10.85	Medium
5	0.022	0.011	1.72E+06	0.455	9.90	Fine
6	0.02	0.01	2.02E+06	0.455	9.81	Very fine

ulations.

Figure 5. Visualization of variation of torque coefficient for different cell counts.

2.1.5. Boundary Layer Analysis and Value of Y$^+$

To accurately resolve the viscous sublayer, which encompasses wall unit *y+*, with a value within 1, a substantial increase in the number of grids is necessary, resulting in a corresponding increase in calculation time. So, the value of y^+, which is considered, is 27.8 as shown in **Figure 6** and this permits the simulation of flow near the propeller surface with a satisfactory level of accuracy.
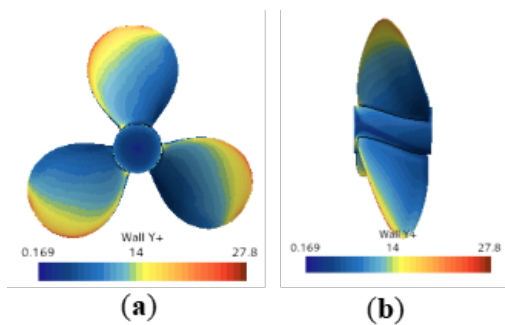

Figure 6. Y+ contour of DTMB 4119 simulation: (**a**) front view, and (**b**) side view at J = 1.089.

2.1.6. Boundary Conditions & Governing Equations

The boundary condition applied at the inlet is the velocity of water having a value of 5.11 m s^{-1}, which remains constant throughout the analysis. The outlet is defined as an outflow boundary condition. A series of angular speed values like 33.532, 28.029, 24.075, 21.094, and 18.766 rev s^{-1} are given to the rotary region containing the propeller for different advance coefficients of 0.625, 0.730, 0.850, 0.97 and 1.089. All the boundaries of the domain, except the inlet and outlet, are assigned walls with no-slip conditions. All the boundary conditions can be visualized in **Figure 7**.
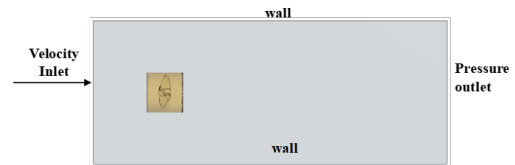

Figure 7. Visualization of boundary conditions for CFD analysis.

Fundamental conservation concepts including the conservation of mass, energy, and momentum govern all fluid motion and transport activities. A fluid model is used to solve these concepts by using partial differential equations. These equations are referred to as the governing equations for fluids from Equations (5)–(8) [26].

$$\frac{\partial \rho}{\partial t} + \frac{\partial}{\partial x_i}\left(\rho u_i\right) = 0 \tag{5}$$

$$\frac{\partial\left(\rho u_i\right)}{\partial t} + \frac{\partial}{\partial x_j}\left(\rho u_i u_j\right) = -\frac{\partial p}{\partial x_i} + \frac{\partial}{\partial x_j}\left(\mu \frac{\partial u_i}{\partial x_j} - \rho\,\overline{u_i' u_j'}\right) + S_i \tag{6}$$

Where ρ is the density of the liquid and u_i is velocity of the fluid, P is the pressure (Pa), S_i is the source term,

μ is the turbulent viscosity, $\rho u_i' u_j'$ is the Reynolds stress term (Pa) and ρ is the liquid density (kg m^{-3}).

The SST k-ω is two-equation eddy viscosity turbulence model and valid for assessing the boundary layer and free flow conditions, being the modified version of both k-ω and k-ε models. The K-ω SST model was chosen for this study due to the presence of adverse pressure gradients and strong curvature regions around the blades of marine propeller DTMB 4119 [27].

Turbulence kinetic energy Equation (7),

$$\frac{\partial}{\partial t}\left(\rho k\right)+\frac{\partial}{\partial x_i}\left(\rho k u_i\right)=\frac{\partial}{\partial x_j}\left(r_k\frac{\partial k}{\partial x_j}\right)+G_K-\mathrm{Y}_K+S_K \tag{7}$$

Specific dissipation rate Equation (8),

$$\frac{\partial}{\partial t}\left(\rho\omega\right)+\frac{\partial}{\partial x_i}\left(\rho\omega u_i\right)=\frac{\partial}{\partial x_j}\left(r\omega\frac{\partial\omega}{\partial x_j}\right)+G_\omega-\mathrm{Y}_\omega+D_\omega+S_\omega \tag{8}$$

Where r_k and Γ_ω are the effective diffusivity of turbulence kinetic energy (k) and specific dissipation rate (ω), respectively, G_K and G_ω are the generation of k and ω, respectively, S_K, S_ω are source terms, Y_K and Y_ω are the dissipation of k and ω respectively and D_ω is the cross-diffusion term.

Solver setting for solution is shown in **Table 3**.

Table 3. Solution and solver setting.

Solver	Implicit Unsteady
Turbulence model	SST K-ω
Pressure velocity coupling scheme	Simple
Time step size	0.001
Number of iterations per step size	3
Total number of iterations	2000

2.1.7. Convergence Criteria

A criterion for convergence, used for simulation, is 10^{-3} as shown in **Figure 8**.
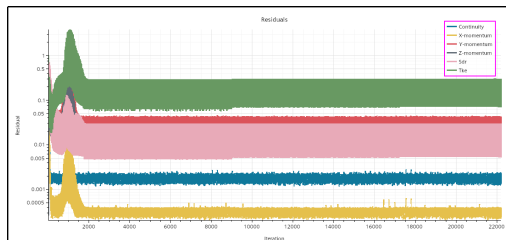

Figure 8. Graphical visualization of residuals.

2.2. Design Modification of DTMB 4119

In this study, rake angle modification of DTMB 4119 is carried out. The rake angle refers to the inclination angle of the propeller blades in relation to the generator line as shown in **Figure 9**. Various DTMB rake angle configurations are presented in **Figure 10**.
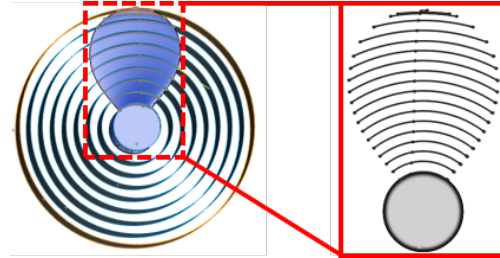

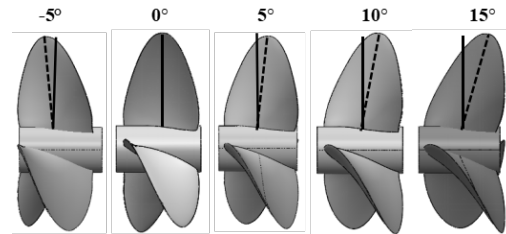**Figure 9.** 3D sectioning of propeller blade.

Figure 10. Modifications of rake angles of DTMB 4119.

3. Results & Discussion

3.1. Validation of CFD Results

The validity of the results is established through a comparison between the open water performance characteristics of the propeller, as calculated using CFD simulation, and the results obtained from EFD. **Figure 11** illustrates that the collective percentage differences between CFD and EFD values range from 0.44% to 9.89%. The percentage error in the thrust coefficient (K_T) ranges from 0.44% to 2.20%, whereas the error in the torque coefficient (K_Q) ranges from 1.20% to 9.86%. The percentage error is observed in the context of open water efficiency, with the error magnitude ranging from 3.17% to 8.62%. Since the values of all percentage errors, especially in the case of efficiency, are below 10%, based on this justification, it can be inferred that the computed outcomes are defensible.
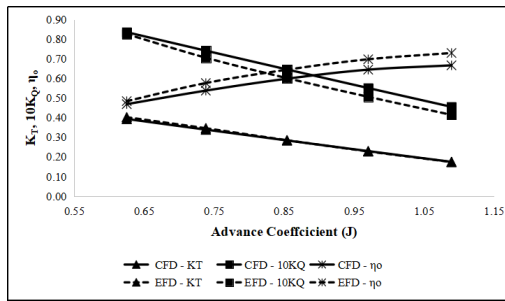
Figure 11. Visualization of comparison between CFD and EFD results.

3.2. Hydrodynamic Analysis

The hydrodynamic analysis is carried out to figure out the performance parameters of the marine propeller which are K_T, K_Q, and η_o. These parameters help in analyzing the open water performance of marine propellers. The results of this analysis are given below.

3.2.1. Open Water Hydrodynamic Performance

The thrust coefficient and torque coefficient are two hydrodynamic coefficients that must be calculated to determine open water performance. Thrust and torque numbers are calculated using a CFD simulation. The graph shown in **Figure 12** clearly demonstrates that the increment in advance coefficient (J) results in a reduction of both thrust coefficient (K_T) and torque coefficient (K_Q) because they are directly proportional to the thrust force and moment, respectively, which decreases as the advance coefficient increases.
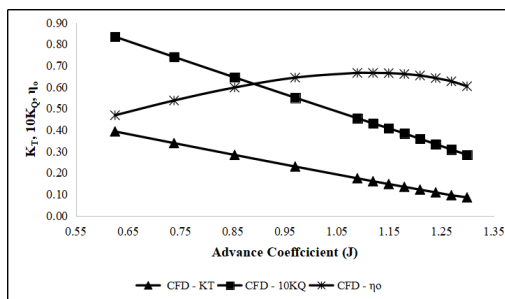

Figure 12. Hydrodynamic performance curves of DTMB 4119.

On the other hand, by raising the value of J, the propeller's open water efficiency (η_o) rises to its maximum value, called maximum efficiency of DTMB 4119, at a specific value of advance coefficient and then decreases, as shown in **Figure 12**. This is because it has a direct re-

lation with the ratio of K_T and K_Q; despite the advance coefficient, the value of this ratio first increases, and then after a specific value of J, which is 1.119, it starts to decrease as the thrust coefficient does not decrease as the torque coefficient does. In short, it can be said that in the case of heavy load conditions (low advance ratio), the propeller exhibits less open water efficiency, while at light conditions (high advance ratio), it manifests an increment in its efficiency.

3.2.2. Open Water Performance and Modification of Rake Angle

- **Thrust Coefficient**

  The plot shown in **Figure 13** manifests that the value of the thrust coefficient decreases as we change the rake angle of DTMB 4119 from 0° to 15°, except for the –5° rake angle. This is because, with an increase in rake angles, the area with higher pressure diminishes. This causes the reduction in thrust force, and as a result, the values of the thrust coefficients minimize. So, the thrust coefficient decreases almost 5% for every positive 5° change in rake angle. Overall, the decrement in thrust coefficient is almost 16% for rake angle modification up to 15°. The value of the thrust coefficient gets increased almost 5% as we change the rake angle to –5°, as the pressure distributed around the blade surface increases.
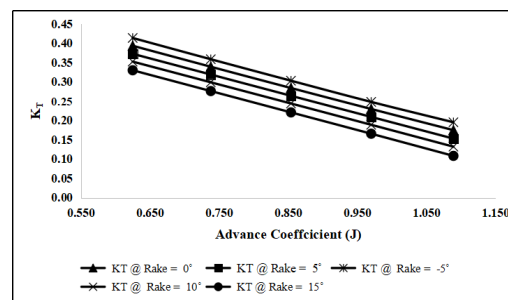

Figure 13. Variation of thrust coefficients of DTMB 4110 propeller for different rake angles.

- **Torque Coefficient**

  Figure 14 depicts that the value of the torque coefficient decreases as we modify the rake angle of DTMB 4119 from 0° to 15°, except for the –5° rake angle. This is because the value of torque required to rotate the propeller decreases as the rake an-

gle increases. So, the torque coefficient decreases almost 5% for every positive 5° modification in the rake angle of DTMB 4119. Overall, the decrement in the torque coefficient is almost 14.8% for rake angle modification up to 15°. The value of the torque coefficient gets increased almost 6% as we change the rake angle to –5°, because the torque to rotate the blades increases.
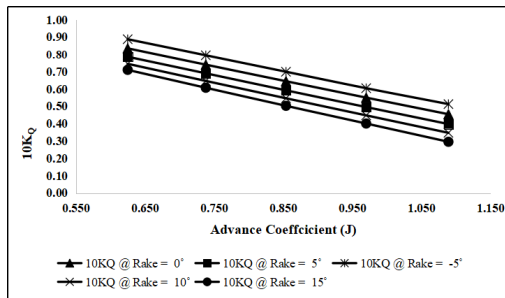

Figure 14. Variation of torque coefficients of DTMB 4110 propeller for different rake angles.

- **Open Water Efficiency**

This graph, shown in **Figure 15**, shows that the increment in the efficiency of DTMB 4119 for the backward rake angles like 5° and 10° is 0.42–1.34% up to J = 0.97 except at J = 1.089 where there is no notable variation in efficiency. The decrement in the efficiency of DTMB 4119 for the higher backward rake angle like 15° is 0.33–1.09% up to J = 0.97 except at J = 1.089 where the diminishing in efficiency is 4.8%. Apart from J = 1.089, where there is zero variation in efficiency, the efficiency of DTMB 4119 decreases by 1.08 to 1.67% at forward rake angles like –5° up to J = 0.97.
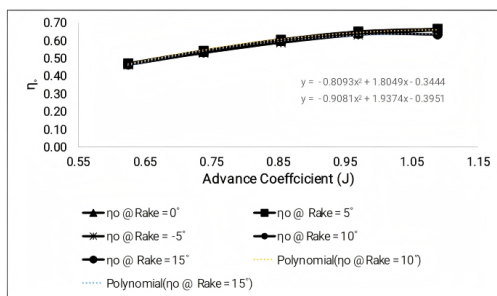

Figure 15. Variation of open water efficiency of DTMB 4110 propeller for different rake angles.

The basic reason behind the rake angle modifica-

tion of the marine propeller is to enhance the clearance distance between the overhang part of the hull stern and the blade tip. Owing to operating in a wake field of the ship hull, propeller working takes place in a field where velocity is continuously varying. So, this may result in an increment of the possibility to transmit pulsating pressure forces to the ship hull. This fact may cause vibrations in the overhanging part at the stern of the ship hull[28]. So, to avoid this, a raking technique is applied. No doubt, raking is beneficial for preventing vibrations according to literature; however, the hydrodynamic performance of marine propellers with this technique needs attention, specifically for DTMB 4119. So, many researchers analyzed the effect of rake angle on the open water efficiency of marine propellers.

Gorji, Ghassemi and Mohamadi[28] investigated the effect of rake angles of 10°, 20° and 30° of DTRC 4119 on its hydrodynamic performance at advance coefficient (J) 0.833 by using CFD technique. They observed that there was a decrement of 17.68% in thrust coefficient and 25.4% in torque coefficient after rake angle modification from 0° to 30°. According to them, the increment in the open water efficiency was 6.4% (60.4% to 64.27%) from 0° to 10°, but it started to diminish by 2.97% (i.e., 64.27% to 62.36%) for rake angles from 10° to 30°. It means that efficiency did not follow a single trend during rake angle modification of DTRC 4119. Anyhow, the overall improvement in the open water efficiency was 3.25% (60.4% to 62.36%) from 0° to 30° of rake angle.

Sajedi and Mahdi[29] investigated the effect of rake angle modification of B3-50 Wageningen B-screw series marine propeller, having a pitch ratio of 1.4, on its open water hydrodynamic performance while operating in uniform and non-uniform flow with non-cavitating and cavitating conditions. In the case of uniform flow with non-cavitating conditions, the investigation revealed that enhancement in the backward rake angles resulted in diminishment of thrust coefficient. It was also observed that at lower rake angles like –5°, the thrust coefficient got enhancement, but the torque coefficient also increased. For example, at advance coefficient J = 0.4, the values of coefficients of thrust and torque were found to be K_T = 0.455, K_Q = 0.100769 respectively for rake an-

gle 15° and K_T = 0.481, K_Q = 0.105653 respectively for rake angle –5°. While the rake angle modification of B3-50 did not have much effect on its efficiency. The values of efficiencies at J = 0.4 were η = 0.2874 and η = 0.2898 for rake angles 15° and –5°, which had negligible differences. It was concluded that the maximum variation in the efficiency for various rake angles was almost 2%, which occurred at higher advance coefficient J = 1.1. In the case of uniform flow with cavitating conditions, the change in the open water hydrodynamic coefficients is negligible due to the rake angle modification. In addition to the above discussion, the non-uniform flow enhances the prominence of rake angle effect on the hydrodynamic performance of the propeller more than that in the case of uniform flow. This means that flow conditions like uniform and non-uniform flow with cavitating or non-cavitating conditions have the potential to alter the impact of rake modification.

Hayati, Hashemi and Shams[30] conducted CFD analysis to examine the effect of rake angles like –5°, 5°, 15° and 20° of B3-50 conventional three-blade b-series propeller, having P/D ratios of 0.6, 0.8 and 1, on its hydrodynamic performance. They observed that the coefficients of torque and thrust values of the propeller are higher with greater backward rake angles like 15° and 20° than those of the propeller with lower ones like –5° and 5°. Anyhow, their analysis revealed that the values of hydrodynamic coefficients augment by changing the rake angle from –5° to 20°, but this augmentation is prominent at heavy load or less advance coefficient J = 0.1. The open water efficiency improves by increasing the rake angles and this change is prominent at light load or high advance ratio J = 0.9. It was also pragmatic that the prominence of alteration in the hydrodynamic parameters was affected by advance coefficient and pitch ratio (P/D).

The comparison of Gorji, Ghassemi and Mohamadi's study with that of Hayati, Hashemi and Shams reveals that the model of the propeller has a significant impact on changing its hydrodynamic performance due to rake angle modification. It is pertinent to mention that the propeller model B350 for Hasan Sajedi and Mahdi[29] and Hayati, Hashemi and Shams[30] are similar; however, the P/D for both studies, when deter-mined, demonstrates tangible differences. Hasan model shows hydrodynamic coefficients decrease, but in Hayati, Hashemi and Shams's study, it increases. These results manifest that the P/D plays an important role in altering hydrodynamic performance due to rake angle modification. So, while analyzing the effect of rake modification on the hydrodynamic coefficients, one must consider factors like uniform & non-uniform flow with cavitating and non-cavitating conditions and the model of the propeller, e.g., DTRC 4119, B-series and INSEAN e779a, etc. It is because these factors can alter the rake modification effect on the hydrodynamic performance of the propeller.

3.2.3. Variation of Transient Pressure on Propeller Blades

For Different Advance in Coefficients

The transient pressure distribution on propeller blades is determined through CFD simulation, utilizing advance coefficients of 0.625, 0.730, 0.83, 0.97, and 1.089. The pressure distribution on the pressure side and suction side of propeller blades at different advance coefficients, mentioned above, is depicted in the corresponding **Figure 16**. The pressure distribution contours indicate that the magnitude of pressure on the pressure side or front side of the blade is greater than that on the suction side or back side of the blade looking from the stern. This pressure difference generates a thrust force that is directed towards the suction surface of the blade and causes the vessel to move forward.

The pressure values corresponding to various advance coefficients are graphically represented in **Figure 17**. The plotted graph effectively demonstrates that there is an inverse correlation between the advance coefficient (J) and the pressure values.

After analyzing the pressure distribution on the front and back sides of the propeller, it is pertinent to observe the wake region with pressure distribution, as shown in **Figure 18**. It is observed that the point of maximum pressure occurs near the tip of the blade and on the pressure side. The locations where the lowest pressure is seen are at the root of the blade and on the suction surface. The region with negative pressure is also witnessed downstream of the hub wake region. At heavy loading conditions, the region of negative pres-

sure is greater than that at light loading conditions. This means that the region of pressure drop diminishes with the increment of advance ratios and this fact leads to a decrement in the strength of vortices as advance ratios increase because negative pressure causes the generation of vortices. Deep observation also reveals that the tip vortices disappear very quickly. It is because, to ascertain the correct value of hydrodynamic coefficients, SST K-ω turbulence model is applied which is a RANS model, and this model is associated with high turbulent kinetic energy.
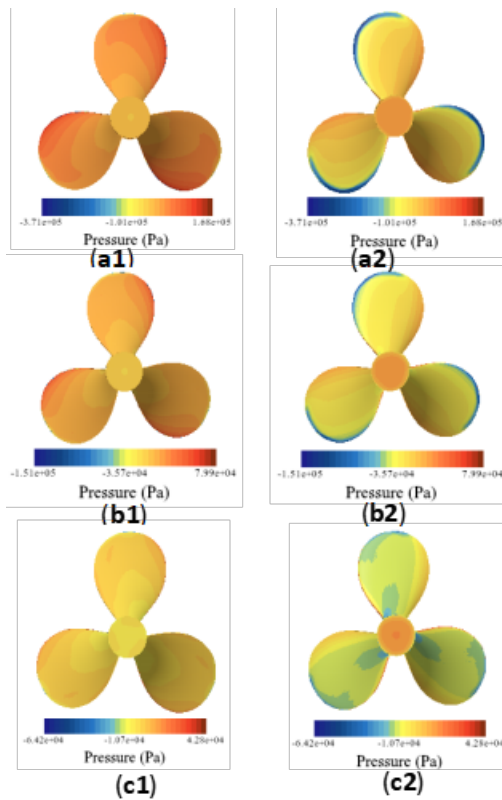

Figure 16. Transient pressure distribution on DTMB 4119 at rake angle = 0°: (**a1**) pressure side, (**a2**) suction side at J = 0.625, (**b1**) suction side, (**b2**) pressure side at J = 0.875, (**c1**) pressure side, and (**c2**) suction side at J = 1.089.
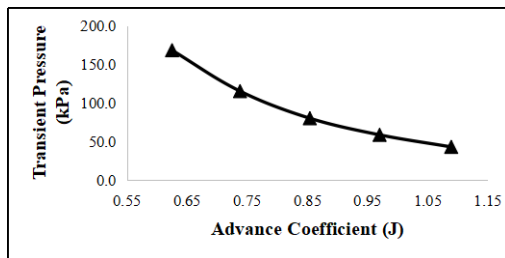

Figure 17. Graphical visualization of transient pressure variation with advance coefficient (J) at rake angle = 0°.
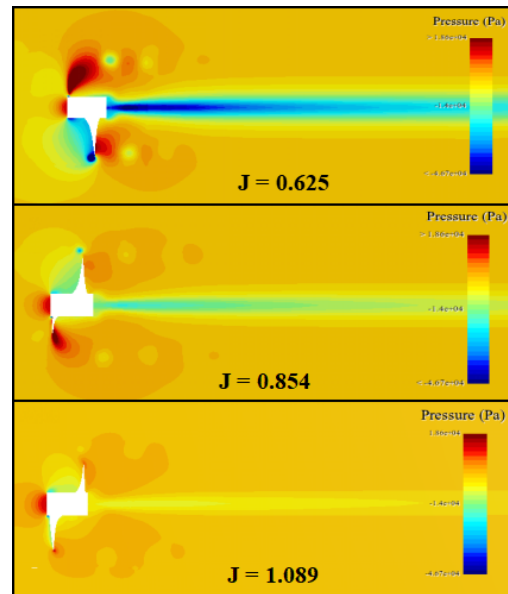

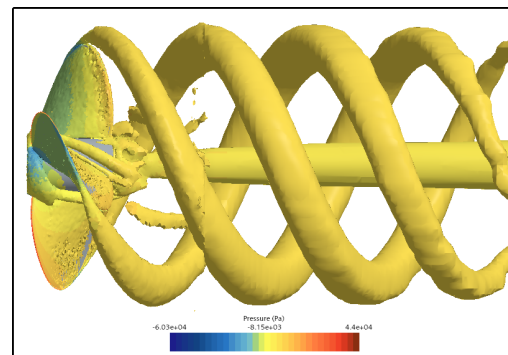**Figure 18.** Visualization of wake behind the propeller at different advance coefficients (J).

Figure 19. Helical configuration of DTMB 4119.

The acceleration of the flow is facilitated by the propeller, wherein each blade induces the formation of a tip vortex that is then conveyed in a backward direction, forming a helical configuration, as shown in **Figure 19**.

4. Conclusions

The concluding remarks of this research study after having performed the hydrodynamic and hydroelastic analysis are listed in the following points.

- The values of thrust and torque coefficients of DTMB 4119 are higher at heavy loading condition (lower advance coefficient) than those at light loading condition (higher advance coefficient). It means both hydrodynamic coefficients diminish as the advance coefficients increase, but the open

water efficiency of DTMB 4119 does not follow this trend. The propeller exhibits less open water efficiency at heavy load condition, while at light condition it manifests an increment in its efficiency up to a specified value of advance ratio.

- In uniform and non-cavitating flow, the rise in backward rake angles such as 5°, 10° and 15° of DTMB 4119 causes its thrust coefficient and torque coefficient to decrease, with the exception of the forward rake angle, –5°, which causes both coefficients to increase. The backward rake angles, 5° and 10°, lead to an improvement of DTMB 4119 efficiency except the rake angles –5° and 15°, which possess different effects on efficiency. The angle –5° diminishes the efficiency of the propeller at its heavy loading condition, except for the negligible variation in its efficiency at light loading conditions, while the angle 15° causes a decrease in efficiency at higher advance coefficients but negligible variation at low advance coefficients. This fact depicts that the rake angles 5° and 10° are suitable for DTMB 4119 operating in uniform and non-cavitating flow.

To analyze further the structure response of DTMB 4119 and its hydrodynamic performance, there are some future recommendations, which are given below, for future research study.

- Future studies can consider enhancing the range of rake angle modification.
- The hydrodynamic analysis of DTMB 4119 can also be carried out in the future by modifying its pitch (P/D) ratio with rake angle modification in uniform flow with only cavitating conditions and non-uniform flow with both cavitating and non-cavitating conditions.

Author Contributions

Supervision of the study, conduction of simulations, formatting and editing the manuscript, A.L.; conduction of validations of simulations, simulations, paper write-up, and editing, S.S.; paper corrections, simulations compilation, editing, I.M.

Funding

Institutional Review Board Statement

Not applicable.

Informed Consent Statement

Not applicable.

Data Availability Statement

Data will be made available on request.

Conflicts of Interest

There are no competing interests between authors regarding this manuscript.

List of Abbreviations

CFD = Computational Fluid Dynamics
SST = Shear Stress Transport
DTMB = David Taylor Model Basin
LL = Lifting Line
LS = Lifting Surface
RANS = Reynolds-Average Navier-Stokes
BEM = Boundary Element Method
EFD = Experimental Fluid Dynamics
RPM = Revolutions Per Minute
MRF = Moving Reference Frame

References

[1] Curam, A.B., Ahmed, E., Rao, M.V. Static and dynamic analyses of a ship propeller. International Journal of Scientific & Engineering Research. 9(3), 1341–1353. Available from: https://www.ijser.org/researchpaper/Static-and-Dynamic-Analyses-of-a-Ship-Propeller.pdf

[2] Elghorab, M., Elwetedy, S., Kotb, A. Open water performance of a marine propeller model using CFD. Proceedings of The International Conference on Fluid Dynamics, ICFD11, At Alexandria, Egypt. Vol

13, Dec. 2013.

[3] Murray, A.B., Korvin-Kroukovsky, B., Lewis, E.V., 1951. Self propulsion tests with small models. SNAME Trcnsnctions. 59, C6.

[4] Cho, J., Lee, S.-C., 1998. Propeller blade shape optimization for efficiency improvement. Computers & Fluids. 27(3), 407–419.

[5] Lerbs, H.W., 1952. Moderately loaded propellers with a finite number of blades and an arbitrary distribution of circulation. Trans Sname. 60, 123–145. Available from: https://repository.tudelft.nl/islandora/object/uuid

[6] Carlton, J., 2018. Marine propellers and propulsion. Butterworth-Heinemann. 2nd edition, pp. 186–192.

[7] Gaggero, S., Brizzolara, S., 2009. Parametric optimization of fast marine propellers via CFD calculations. Proceedings of the 10th International Conference on Fast Sea Transportation; Athens, Greece, Oct. 2009.

[8] Ekinci, S., Celik, F., Guner, M., 2010. A practical noise prediction method for cavitating marine propellers. Brodogradnja: Teorija i Praksa Brodogradnje i Pomorske Tehnike. 61(4), 359–366.

[9] Krasilnikov, V., Sun, J., Halse, K.H., 2009. CFD investigation in scale effect on propellers with different magnitude of skew in turbulent flow. Proceedings of The First International Symposium on Marine Propulsors; (June 22 –June 24 2009); Trondheim, Norway. pp. 25–40.

[10] Funeno, I., 2002. Analysis of unsteady viscous flows around a highly skewed propeller. Journal of Kansai Society of Naval Architects. 237, 39–45. (in Japanese). Available from: https://jglobal.jst.go.jp/en/detail?JGLOBAL_ID=200902151831528770

[11] Amoraritei, M., 2005. Application of CFD in analysis of conventional propeller and azimuth thruster. Scientific Bulletin of the 'Politehnica'University of Timisoara, Transactions on Mechanics. Vol. 50, 2005.

[12] Ebrahimi, A., Seif, M.S., Nouri-Borujerdi, A., 2019. Hydro-acoustic and hydrodynamic optimization of a marine propeller using genetic algorithm, boundary element method, and FW-H equations. Journal of Marine Science and Engineering. 7(9), 321.

[13] Yari, E., Ghassemi, H., 2016. Hydrodynamic analysis of the surface-piercing propeller in unsteady open water condition using boundary element method, International Journal of Naval Architecture and Ocean Engineering. 8(1), 22–37. DOI: https://doi.org/10.1016/j.ijnaoe.2015.09.002

[14] Boumediene, K., Belhenniche, S., Imine, O., et al., 2019. Computational hydrodynamic analysis of a highly skewed marine propeller. Journal of Naval Architecture & Marine Engineering. 16(1).

[15] Saha, G.K., Maruf, M.H.I., Hasan, M.R., 2019. Marine propeller modeling and performance analysis using CFD tools. AIP Conference Proceedings. 2121(1). DOI: https://doi.org/10.1063/1.5115883

[16] Guo, H.-p., Zou, Z.-j., Wang, F., et al., 2019. Numerical investigation on the hydrodynamic characteristics of a marine propeller operating in oblique inflow. Applied Ocean Research. 93, 101969. DOI: https://doi.org/10.1016/j.apor.2019.101969

[17] Bouregba, F., Belkadi, M., Aounallah, M., et al., 2019. Effect of the blade number on the marine propeller performance. EPJ Web of Conferences. 213, 02007.

[18] Hu, X.-f., Huang, Z.-y., Hong, F.-w., 2009. Unsteady hydrodynamics forces of propeller predicted with viscous CFD. Chinese Journal of Hydrodynamics. 24(6), 734–739.

[19] Huang, S., Zhu, X.-y., Guo, C.-y., et al., 2007. CFD simulation of propeller and rudder performance when using additional thrust fins. Journal of Marine Science and Application. 6, 27–31.

[20] Mirjalili, S., Lewis, A., Mirjalili, S.A.M., 2015. Multi-objective optimisation of marine propellers. Procedia Computer Science. 51, 2247–2256. DOI: https://doi.org/10.1016/j.procs.2015.05.504

[21] Martínez-Calle, J.n., Balbona-Calvo, L., González-Pérez, J., et al., 2002. An open water numerical model for a marine propeller: A comparison with experimental data. Fluids Engineering Division Summer Meeting. 36169, 807–813. Available from: https://api.semanticscholar.org/CorpusID:109382751

[22] Watanabe, T., Kawamura, T., Takekoshi, Y., et al., 2003. Simulation of steady and unsteady cavitation on a marine propeller using a RANS CFD code. Proceedings of The Fifth International Symposium on Cavitation; (Nov. 1–Nov.4,2003), (Osaka, Japan). Available from: https://api.semanticscholar.org/CorpusID:62883924

[23] Rhee, S.H., Koutsavdis, E., 2005. Two-dimensional simulation of unsteady marine propulsor blade flow using dynamic meshing techniques. Computers & Fluids. 34(10), 1152–1172. DOI: https://doi.org/10.1016/j.compfluid.2004.09.005

[24] Ghasemi, H., 2009. The effect of wake flow and skew angle on the ship propeller performance. Scientia Iranica. 16(2), 149–158.

[25] Krasilnikov, V., Ponkratov, D., Crepier, P., 2011. A numerical study on the characteristics of the system propeller and rudder at low speed operation. Proceedings of the Second International Symposium on Marine Propulsors; Hamburg, Germany; June 2011; pp. 157–168.

[26] Raja, R.S., 2012. Coupled fluid structure interaction analysis on a cylinder exposed to ocean

wave loading [Master's thesis]. Göteborg, Sweden: Chalmers University of Technology. pp. 1–55. Available from: https://odr.chalmers.se/server /api/core/bitstreams/5e52d3e3-bb6c-4955-a 740-ec4b27d113ed/content

[27] Hassan, T., Islam, M.T., Rahman, M.M., et al., 2022. Evaluation of different turbulence models at low reynolds number for the flow over symmetric and cambered airfoils. Journal of Engineering Advancements. 3(1), 12–22. DOI: https://doi.org/10.38032/jea.2022.01.003

[28] Gorji, M., Ghassemi, H., Mohamadi, J., 2019. Effect of rake and skew on the hydrodynamic characteristics and noise level of the marine propeller. Iranian Journal of Science and Technology, Transactions of Mechanical Engineering. 43, 75–85. DOI: https://doi.org/10.1007/s40997-017-0108-y

[29] Sajedi, H., Mahdi, M., 2019. Numerical investigation of the rake angle effect on the hydrodynamic performance of propeller in a uniform and nonuniform flow. Proceedings of The Institution of Mechanical Engineers, Part C: Journal of Mechanical Engineering Science. 233(18), 6326–6338. DOI: https://doi.org/10.1177/0954406219830136

[30] Hayati, A., Hashemi, S., Shams, M., 2012. A study on the effect of the rake angle on the performance of marine propellers. Proceedings of the Institution of Mechanical Engineers, Part C: Journal of Mechanical Engineering Science. 226(4), 940–955. DOI: https://doi.org/10.1177/0954406211418588